A Multiscale Model for the Electrochemical Reactions in LSCF Based Solid Oxide Cell

Supporting Information

Linjian Ma[a], Pikee Priya[a] and N.R. Aluru[a,*]

[a] Department of Mechanical Science and Engineering, Beckman Institute for Advanced Science and Technology, University of Illinois at Urbana-Champaign, Urbana, Illinois 61801, USA

S1: Details on the steps of the entire oxygen reduction process

S2: Discussion on interface structure

S3: Details on the expressions for G(T)

S4: Derivation of the expression for the electric field

S5: Details on the definitions for interface and subsurface layers

S6: Detailed parameter values used in the simulations

S7: Detailed DFT+U calculation results of optimized structures and energy barriers

S8: Influence of vacancy concentration on reaction rate constants and diffusivities

S1: Details on the steps of the entire oxygen reduction process

The entire oxygen reduction process can be separated into five transport steps (T1 to T5), and six reaction steps (R1 to R6) and are presented below:

1. Transport of O_2 in the gas phase. (T1)
2. Adsorption of O_2 on the LSCF surface to form excited O_{2O}^{x} molecule. (R1)
3. Transport of the adsorbed O_{2O}^{x} on the LSCF surface. (T2)
4. Adsorbed O_{2O}^{x} fills vacancies on the Fe/CoO layer of the LSCF surface: (R2)
5. Transport of peroxo, $O_{2O}^{''}$ species on the LSCF surface. (T3)
6. Splitting of peroxo, $O_{2O}^{''}$ into two oxo, $O_O^{'}$ species on the LSCF surface. (R3)
7. Transport of oxo, $O_O^{'}$ species on the LSCF surface. (T4)
8. Transport of $O_O^{'}$ from the surface LSCF to the bulk LSCF: (R4)
9. Transport of oxide, $O_O^{''}$ ions in bulk LSCF. (T5)
10. Transport of $O_O^{''}$ ion across the interface between LSCF and electrolyte: (R5)
11. Transport of peroxo, $O_{2O}^{''}$ species at the surface of LSCF across the air/LSCF/GDC TPB:(R6)

A more detailed description of the notation used in the above chemical reaction steps and other equations is shown in Table S1-1.

Table S1-1. A detailed description of the notation

O_{2O}^{x}	Excited O_2^* molecule at an anionic O site (neutral) on LSCF surface
$O_{2O}^{''}$	O_2^{2-} at an anionic O site on LSCF surface
$O_O^{'}$	O^{-} at an anionic O site in LSCF
$O_O^{''}$	O^{2-} at an anionic O site in LSCF/GDC
k	Reaction rate constant
D	Diffusivity
k_B	Boltzmann constant

T	Temperature
C	Concentration of different species
h	Planck's constant
G	Gibbs free energy
λ	Jump length of a diffusion step
z	Number of first neighbors in the diffusion step, which is 2 in 1D diffusion, 4 on a square lattice, and 6 on a hexagonal lattice
F	Helmholtz free energy
P	Pressure of gas
V	Volume of the gas
I_m	Moment of inertia of one molecule
Z	Partition function
v	Vibrational frequency
E_0	Electronic internal energy at 0K
S	Entropy
ϕ	Porosity
τ	Tortuosity
r	Reaction rates for different reaction steps
φ	Electric potential
suf	Reactions that happen on the LSCF surface
TPB	Reactions that happen on LSCF/GDC/gas triple phase boundaries
int	Reactions that happen on LSCF/GDC interface
σ	Electronic conductivity of LSCF
A_{suf}	LSCF surface area per unit volume
A_{int}	The percentage of LSCF/GDC contacting surface area on the interface
A_{TPB}	TPB length per unit interface area
$C_{O^{2-}}^{max}$	Concentration of oxygen lattice sites, about 83147 mol/m^3
$C_{O_{suf}^{2-}}^{max}$	Concentration of surface oxygen lattice sites, about 10^{-5} mol/m^2
F_a	Faraday's constant
I	Current density
I_{TPB}	Current density across the triple phase boundary
I_{int}	Current density across the LSCF/GDC interface
η	Overpotential at LSCF/GDC interface
$\Delta G_{f,vac}$	Vacancy formation free energy
$\Delta G_{f,vac}^{perf}$	Vacancy formation free energy with no vacancies in the lattice
a	The parameter representing the free energy deviation from the ideal structure

γ_{bulk}	The parameter representing the deviation of $\Delta G_{D_{O^{2-}}}$ attributed to C_{V_O} variations
γ_{suf}	The parameter representing the deviation of $\Delta G_{k_{3,suf}}$ attributed to C_{V_O} variations
χ	The electrostatic potential step at the LSCF/gas interface
e	Charge of an electron
α	Charge transfer coefficient
Cap_{suf}	Capacitance for surface LSCF
d	Vertical distance between the uppermost oxygen and the surface layer
ε	Permittivity of the material
S_e	Sensitivity of current density
P_a	Parameters in sensitivity analysis

S2: Discussion on interface structure

Unlike the interface structure with (100) terminated LSCF and (100) terminated CeO_2, which is shown in Fig. 3(e), the interface structure with (100) terminated LSCF and (110) terminated CeO_2 is not a stable structure. We can see from Fig. S2-1(b) that the relaxed interface has a significant distortion on the SrO layer compared to the bulk LSCF structure, and the distance between interface SrO layer and the CeO_2 layer is much larger than the distance between other neighboring layers, indicating that this interface structure is not favorable.

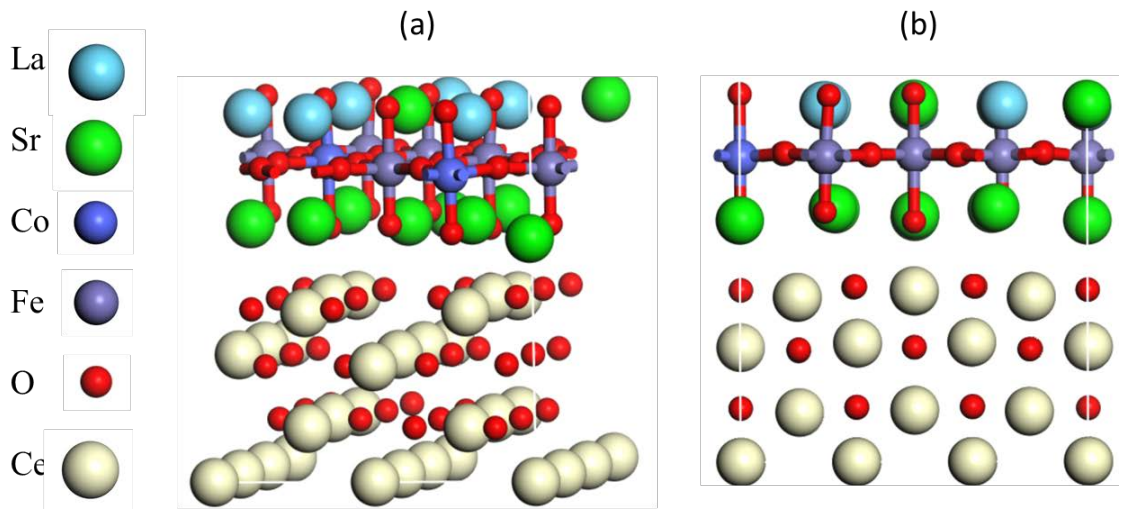

Fig. S2-1 Two side views of the LSCF / CeO_2 interface structure with (100) terminated LSCF and (110) terminated CeO_2.

S3: Details on the expressions for G(T)

For the O_2 molecules in the gas phase, the Gibbs free energy is expressed as

$$G(T) = F^{0K} + F^{translation} + F^{rotation} + F^{vibration} + PV$$

$$= -k_B T\, ln(Z^{0K}) - k_B T\, ln(Z^{tr}) - k_B T\, ln(Z^{rot}) - k_B T\, ln\left(Z^{vib}\right) + PV$$

$$Z^{0K} = 3\, exp\left(-\frac{E_0}{k_B T}\right)$$

$$Z^{tr} = \left(\frac{2\pi m k_B T}{h^2}\right)^{\frac{3}{2}} V$$

$$Z^{rot} = \frac{8\pi^2 I_m k_B T}{2h^2}$$

$$Z^{vib} = \frac{exp(-\frac{h\nu_{O_2}}{2k_B T})}{1-exp(-\frac{h\nu_{O_2}}{k_B T})} \qquad \text{(S3-1)}$$

Derivations of these equations are from reference 1.

For the adsorbed O_2 molecule, the Gibbs free energy can be expressed as

$$G_{ads}(T) = F_{ads} + PV$$

$$F_{ads} = (E - TS)_{ads} = (E_0)_{ads} - TS_{ads} + \frac{7}{2}k_B T \quad \text{(S3-2)}$$

For the adsorbed O_2 gas, the following approximations are used to obtain the entropy term S_{ads}[2,3]:

$$S_{ads} \approx 0.7S - 3.3k_B$$

$$S = \frac{1}{T}(E_0 + \frac{7}{2}k_B T - F) \quad \text{(S3-3)}$$

For the oxide ions (O_O'', O_{2_O}'' and O_O''), the Gibbs free energy can be expressed as

$$G_i(T) \approx F_i = F_i^{0K} + F_i^{vibration}$$

$$F_i^{0K} = E_{0,i}$$

$$F_i^{vibration} = \frac{1}{2}\sum_{m=1}^{3N} hv_m + k_B T \sum_{m=1}^{3N} ln(1 - exp(-\frac{hv_m}{k_B T})) \quad (S3-4)$$

The term $E_{0,i}$ is the internal energy of each species at 0 K. These terms are calculated using DFT+U calculations.

The vibrational frequencies are calculated using the finite displacement method. All oxygen atoms in the reaction or diffusion process and the nearest neighbor atoms were included in the calculations, as they are directly involved in the reaction mechanism[4]. The vibrational frequencies at a constant volume were obtained within the harmonic approximation using finite ionic displacements ±0.015Å.

S4: Derivation of the expression for the electric field

The current density distribution is presented in Fig. S4-1. At the top boundary, the ionic current density is 0, and the overall current density is from the electronic conduction. At the bottom

boundary, the overall current density is from the ionic conduction. According to the current density conservation equation, we have,

$$I(O^{2-}) + I(e^{-}) = I = I(O^{2-})(\text{bottom}) \tag{S5-1}$$

where

$$I(e^{-}) = -\sigma \frac{d}{dz}\varphi \tag{S5-2}$$

$$I(O^{2-}) = 2F_a D_{O^{2-}} \left(\frac{d}{dz} C_{O^{2-}} - \frac{2F_a C_{O^{2-}}}{RT} \frac{d}{dz}\varphi \right) \tag{S5-3}$$

$$I(O^{2-})(bottom) = 2F_a D_{O^{2-}} \frac{d}{dz} C_{O^{2-}}(bottom) \tag{S5-4}$$

After putting (S5-2~S5-4) into (S5-1), we can get

$$-\frac{\mathrm{d}}{\mathrm{dz}}\varphi = \frac{-2\mathrm{F_a D_{O^{2-}}}(\frac{\mathrm{d}}{\mathrm{dz}}\mathrm{C_{O^{2-}}} - \frac{\mathrm{d}}{\mathrm{dz}}\mathrm{C_{O^{2-}}(bottom)})}{\sigma + \frac{4\mathrm{F_a}^2 \mathrm{C_{O^{2-}} D_{O^{2-}}}}{\mathrm{RT}}} \tag{S4-3}$$

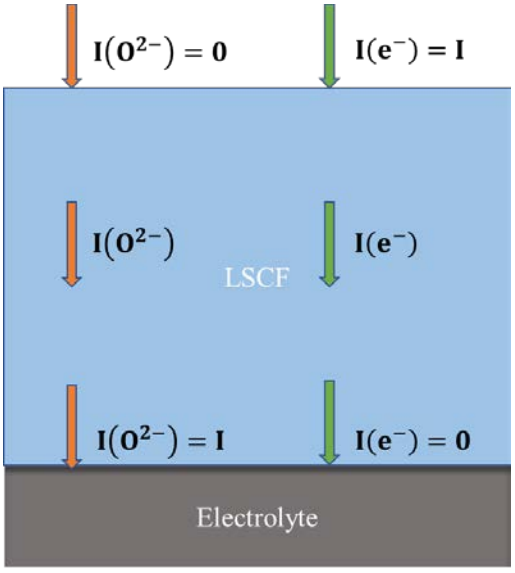

Fig. S4-1 Schematic representation of current density distribution in LSCF. $I(O^{2-})$ is the current density from oxide ion conduction, and $I(e^{-})$ is the current density from electronic conduction.

S5: Details on the definitions of interface and subsurface layers

The positions for different oxide ions and vacancies are presented in Fig. S5-1. Because oxide ions can only migrate from one layer to its adjacent layer, the reactions (R4) and (R5) consist of multiple migration steps across different layers. As to the LSCF surface structure, the 4th atom layer (Fig. S5-1(a)) is regarded as the bulk layer. As to the interface structure, the 1st atom layer (Fig. S5-1(b)) is considered to be the LSCF bulk layer, the 7th atom layer (Fig. S5-1(b)) is considered to be the electrolyte bulk layer, and all the other layers in between are considered to be the interfacial layers.

The reaction rate expressions for the migration of oxide ions from the surface to the bulk are as follows:

$$r_{R4}^{suf\rightarrow sub\_1} = A_{suf}\left\{k_{R4\_1}^{+} C_{O_{suf}^{-}} \frac{C_{V_O^{sub\_1}}}{C_{O_{suf}^{2-}}^{max}} - k_{R4\_1}^{-} C_{O_{sub\_1}^{2-}} \frac{C_{V_O^{suf}}}{C_{O_{suf}^{2-}}^{max}}\right\} \tag{S5-1}$$

$$r_{R4}^{sub\_1\rightarrow sub\_2} = A_{suf}\left\{k_{R4\_2}^{+} C_{O_{sub\_1}^{2-}} \frac{C_{V_O^{sub\_2}}}{C_{O_{suf}^{2-}}^{max}} - k_{R4\_2}^{-} C_{O_{sub\_2}^{2-}} \frac{C_{V_O^{sub\_1}}}{C_{O_{suf}^{2-}}^{max}}\right\} \tag{S5-2}$$

$$r_{R4}^{sub\_2\rightarrow bulk} = A_{suf}\left\{k_{R4\_3}^{+} C_{O_{sub\_2}^{2-}} \frac{C_{V_O}}{C_{O^{2-}}^{max}} - k_{R4\_3}^{-} C_{O^{2-}} \frac{C_{V_O^{sub\_2}}}{C_{O^{2-}}^{max}}\right\} \tag{S5-3}$$

where suf → sub_1 denotes the migration of oxide ions from the surface to the first subsurface layer, sub_1 → sub_2 denotes the migration of oxide ions from the first subsurface layer to the second subsurface layer, and sub_2 → bulk denotes the migration of oxide ions from the second subsurface layer to the bulk. When the reactions reach the steady state, we have

$$r_{R4}^{suf\rightarrow sub\_1} = r_{R4}^{sub\_1\rightarrow sub\_2} = r_{R4}^{sub\_2\rightarrow bulk} = r_{R4}^{suf} \tag{S5-4}$$

The values for $C_{V_O^{sub\_1}}$ and $C_{O_{sub\_1}^{2-}}$ can be obtained after solving equation (S5-4).

The reaction rate expressions for the migrations of oxide ions across the LSCF/GDC interface are as follows:

$$r_{R5}^{bulk\to int\_1} = A_{int}\left\{k_{R5\_1}^{+} C_{V_O^{int\_1}} \frac{C_{O^{2-}}}{C_{O^{2-}}^{max}} - k_{R5\_1}^{-} C_{O_{int\_1}^{2-}} \frac{C_{V_O}}{C_{O^{2-}}^{max}}\right\} \quad \text{(S5-5)}$$

$$r_{R5}^{int\_1\to int\_2} = A_{int}\left\{k_{R5\_2}^{+} C_{V_O^{int\_2}} \frac{C_{O_{int\_1}^{2-}}}{C_{O^{2-}}^{max}} - k_{R5\_2}^{-} C_{O_{int\_2}^{2-}} \frac{C_{V_O^{int\_1}}}{C_{O^{2-}}^{max}}\right\} \quad \text{(S5-6)}$$

$$r_{R5}^{int\_2\to int\_3} = A_{int}\left\{k_{R5\_3-}^{+} C_{V_O^{int\_3}} \frac{C_{O_{int\_2}^{2-}}}{C_{O^{2-}}^{max}} - k_{R5\_3}^{-} C_{O_{int\_3}^{2-}} \frac{C_{V_O^{int\_2}}}{C_{O^{2-}}^{max}}\right\} \quad \text{(S5-7)}$$

$$r_{R5}^{int\_3\to int\_4} = A_{int}\left\{k_{R5\_4}^{+} exp\left(\frac{-2F_a\eta}{RT}\right) C_{V_O^{int\_4}} \frac{C_{O_{int\_3}^{2-}}}{C_{O^{2-}}^{max}} - k_{R5\_4}^{-} C_{O_{int\_4}^{2-}} \frac{C_{V_O^{int\_3}}}{C_{O^{2-}}^{max}}\right\} \quad \text{(S5-8)}$$

$$r_{R5}^{int\_4\to int\_5} = A_{int}\left\{k_{R5\_5}^{+} C_{V_O^{int\_5}} \frac{C_{O_{int\_4}^{2-}}}{C_{O^{2-}}^{max}} - k_{R5\_5}^{-} C_{O_{int\_5}^{2-}} \frac{C_{V_O^{int\_4}}}{C_{O^{2-}}^{max}}\right\} \quad \text{(S5-9)}$$

$$r_{R5}^{int\_5\to ele} = A_{int}\left\{k_{R5\_6}^{+} C_{V_O^{ele}} \frac{C_{O_{int\_5}^{2-}}}{C_{O^{2-}}^{max}} - k_{R5\_6}^{-} C_{O_{ele}^{2-}} \frac{C_{V_O^{int\_5}}}{C_{O^{2-}}^{max}}\right\} \quad \text{(S5-10)}$$

where bulk → int_1 denotes the migration of oxide ions from bulk LSCF to the first interfacial layer, int_i → int_j denotes the migration of oxide ions from the ith interfacial layer to the jth interfacial layer, and int_5 → ele denotes the migration of oxide ions from the fifth interfacial layer to the bulk electrolyte. The overpotential η is added to the reaction rate $r_{R5}^{int\_3\to int\_4}$, for the third and fourth interfacial layers are the boundaries for LSCF and GDC, respectively, and the interface electric double layer induced overpotential acts between them. When the reactions reach the steady state, we have

$$r_{R5}^{bulk\to int\_1} = r_{R5}^{int\_1\to int\_2} = r_{R5}^{int\_2\to int\_3} = r_{R5}^{int\_3\to int\_4} = r_{R5}^{int\_4\to int\_5} = r_{R5}^{int\_5\to ele} = r_{R5}^{int} \quad \text{(S5-11)}$$

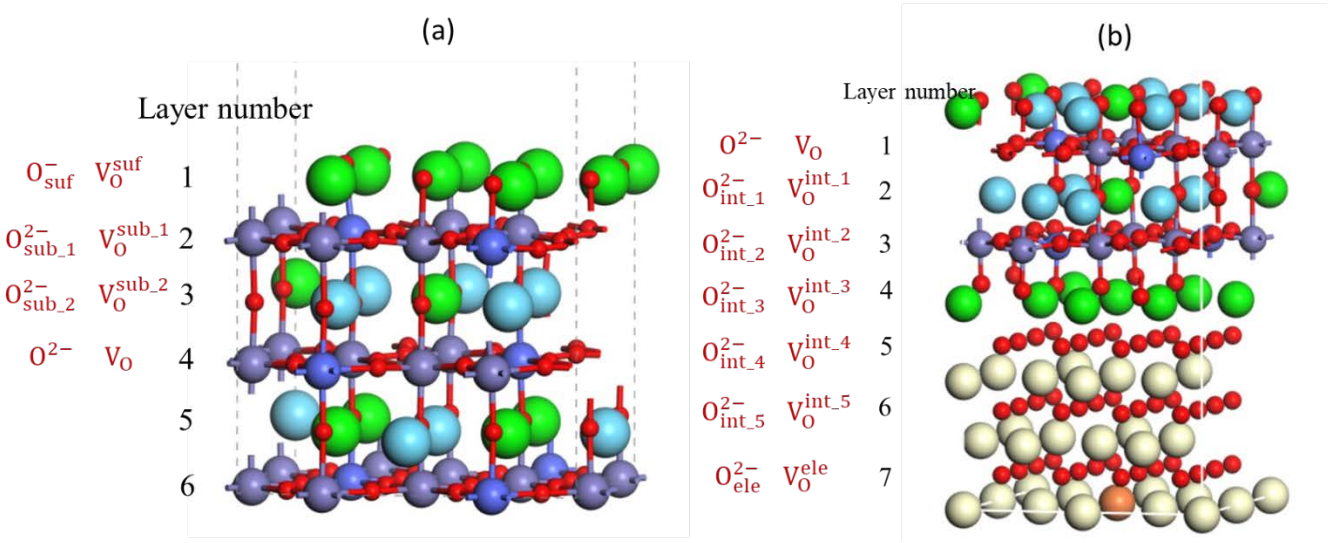

Fig. S5-1 Schematic representation of the position of oxide ions and vacancies in the different subsurface and interfacial layers.

The values for $C_{V_O^{int\_1}}$ and $C_{O^{2-}_{int\_1}}$ can be obtained after solving equation (S5-11).

S6: Detailed Parameter Values used in the Simulations

Table S6-1. Internal energy barriers and free energy barriers for each reaction rate constant. Here $\Delta E(0)$ is the internal energy barrier calculated from DFT+U calculations at 0K. $\Delta G(T) - \Delta E(0)$ is part of the free energy barrier coming from nonzero temperature. $\Delta G(T)$ is the free energy barrier at temperature T. Here T=1073K.

Parameters	$\Delta E(0)$(eV)	$\Delta G(T) - \Delta E(0)$(eV)	$\Delta G(T)$(eV)	Values (s^{-1})
k^+_{R1}	-0.7	1.134	0.434	2.06×10^{11}
k^-_{R1}	0	0	0	2.23×10^{13}
k^+_{R2}	-0.615	0.736	0.121	6.06×10^{12}
k^-_{R2}	0	0	0	2.23×10^{13}
k^+_{R3}	0.638	0.161	0.799	3.38×10^{9}
k^-_{R3}	1.24	0.190	1.43	4.1×10^{6}
$k^+_{R4\_1}$	0	0	0	2.23×10^{13}
$k^-_{R4\_1}$	1.17	-0.096	1.074	2.04×10^{8}
$k^+_{R4\_2}$	1.94	-0.032	1.908	2.50×10^{4}
$k^-_{R4\_2}$	0	0	0	2.23×10^{13}

$k^{+}_{R4\_3}$	0	0	0	2.23×10^{13}
$k^{-}_{R4\_3}$	1.316	-0.032	1.284	2.12×10^{7}
$k^{+}_{R5\_1}$	0	0	0	2.23×10^{13}
$k^{-}_{R5\_1}$	0.681	0	0.681	1.43×10^{10}
$k^{+}_{R5\_2}$	1.452	0.082	1.534	1.41×10^{6}
$k^{-}_{R5\_2}$	0	0	0	2.23×10^{13}
$k^{+}_{R5\_3}$	0.7	0.146	0.846	2.41×10^{9}
$k^{-}_{R5\_3}$	0.706	0	0.706	1.09×10^{10}
$k^{+}_{R5\_4}$	1.369	0.145	1.514	1.76×10^{6}
$k^{-}_{R5\_4}$	0	0	0	2.23×10^{13}
$k^{+}_{R5\_5}$	0	0	0	2.23×10^{13}
$k^{-}_{R5\_5}$	1.799	0	1.799	8.14×10^{4}
$k^{+}_{R5\_6}$	0	0	0	2.23×10^{13}
$k^{-}_{R5\_6}$	0.530	0	0.530	7.30×10^{10}

Table S6-2. Internal energy barriers and free energy barriers for diffusivities. Here λ is the migration length. The value for $D_{O^{2-}}$ is from experiments, and the value for D_{O_2} is from Dusty Gas Model[6].

Parameters	Place	$\Delta E(0)$(eV)	$\Delta G(T) - \Delta E(0)$(eV)	$\Delta G(T)$(eV)	λ(Å)	Values (m^2s^{-1})
$D_{O^{2-}}$[7]	Bulk LSCF	/	/	/	/	$[9.73,15.85]\times 10^{-10}$
D_{O_2}[6]	Gas phase	/	/	/	/	1.2×10^{-5}
$D_{O_2^*}$	LSCF surface	0	0	0	3.843	8.25×10^{-7}
$D_{O_2^{2-}}$	LSCF surface	1.162	0.116	1.279	1.922	2.06×10^{-13}
D_{O^-}	LSCF surface	2.99	0.098	3.088	3.843	2.69×10^{-21}

Table S6-3. LSCF electrode microstructural parameters. The values presented below are from Reference 6.

A_{suf}	$5\mu m^2/\mu m^3$
A_{TPB}	$3.4\mu m/\mu m^2$
A_{int}	$0.6\mu m^2/\mu m^2$
ϕ_{gas}	0.4
ϕ_{LSCF}	0.6
τ_{gas}, τ_{LSCF}	1.46

Table S6-4. Parameters used in $\Delta G(C)$ expressions.

Parameters	Experimental Value
a[8]	[9.2,10.86] eV
γ_{bulk}[7]	0.37
γ_{suf}[7]	0.56
ε_{LSCF}[9,10]	11.068

S7: Detailed DFT+U calculation results of optimized structures and energy barriers

The details of reaction R1~R5 are shown in Fig S7-1~S7-5, respectively. The brown circles denote the moving oxygen atoms.

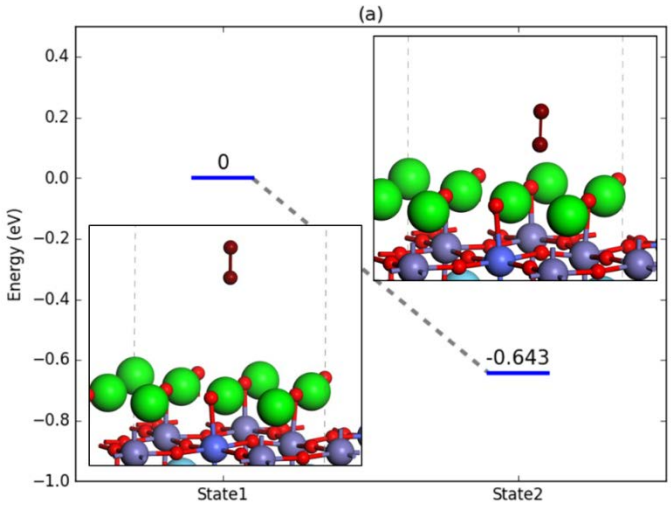

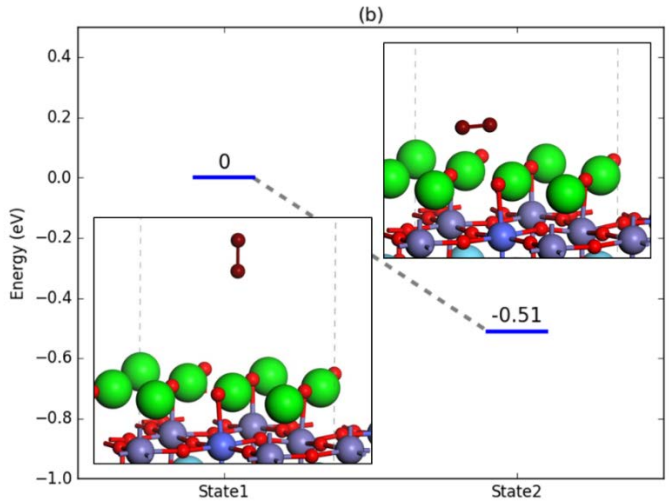

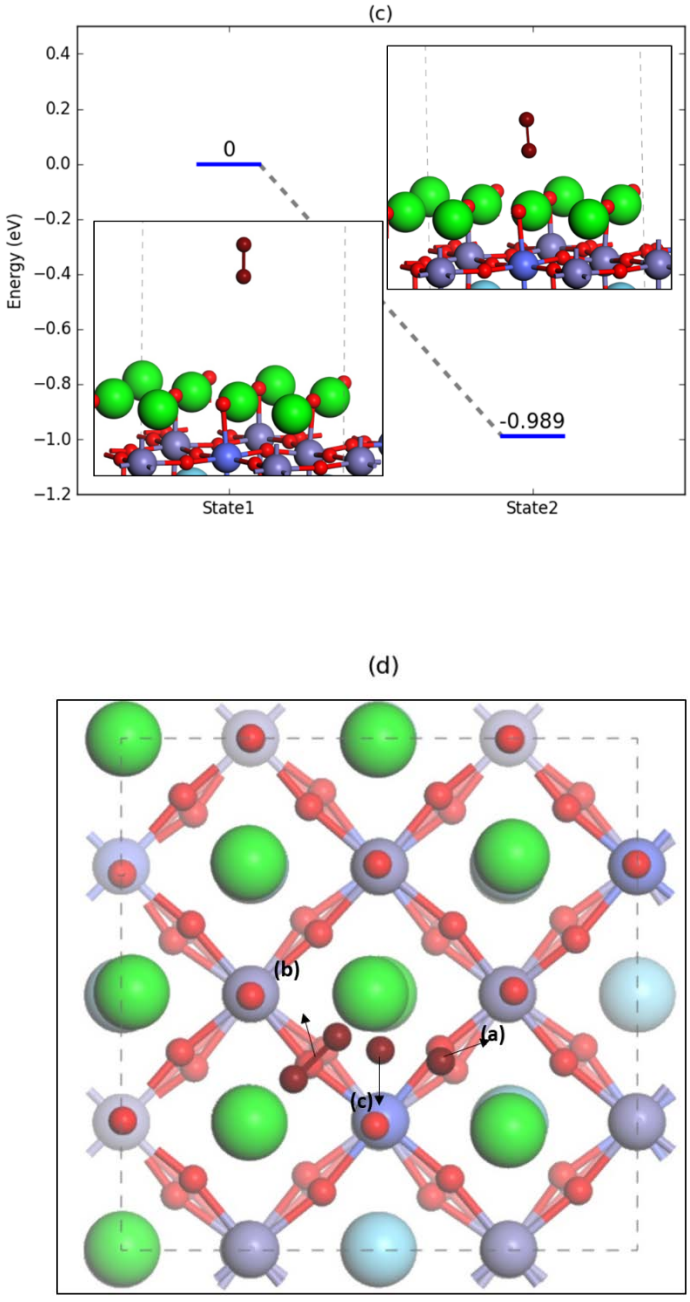

Fig. S7-1 Energy profile for reaction R1. (a-c) The energy profiles with three different final optimized structures. The energy difference used in Table S6-1 is the average value of these three results. (d) Top view of the adsorbed oxygen molecule on the LSCF surface.

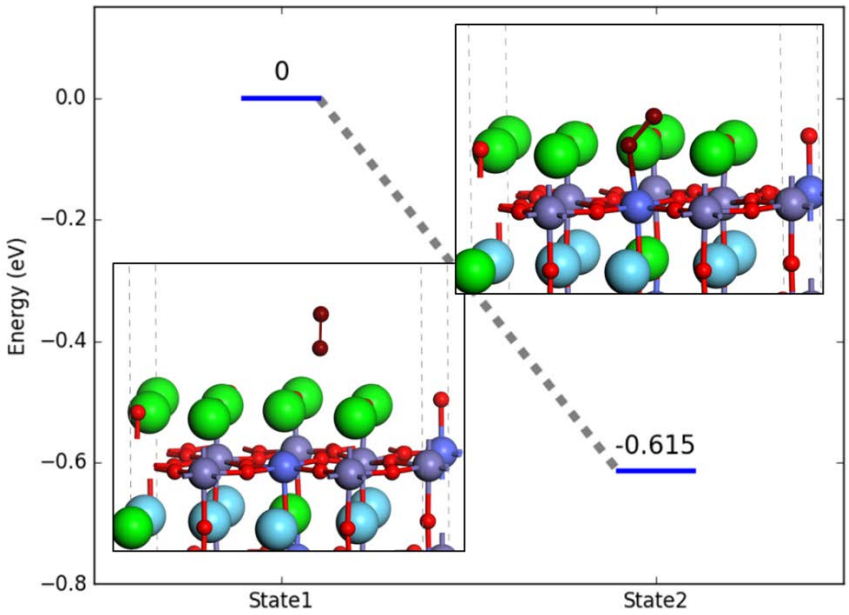

Fig. S7-2 Energy profile for reaction R2.

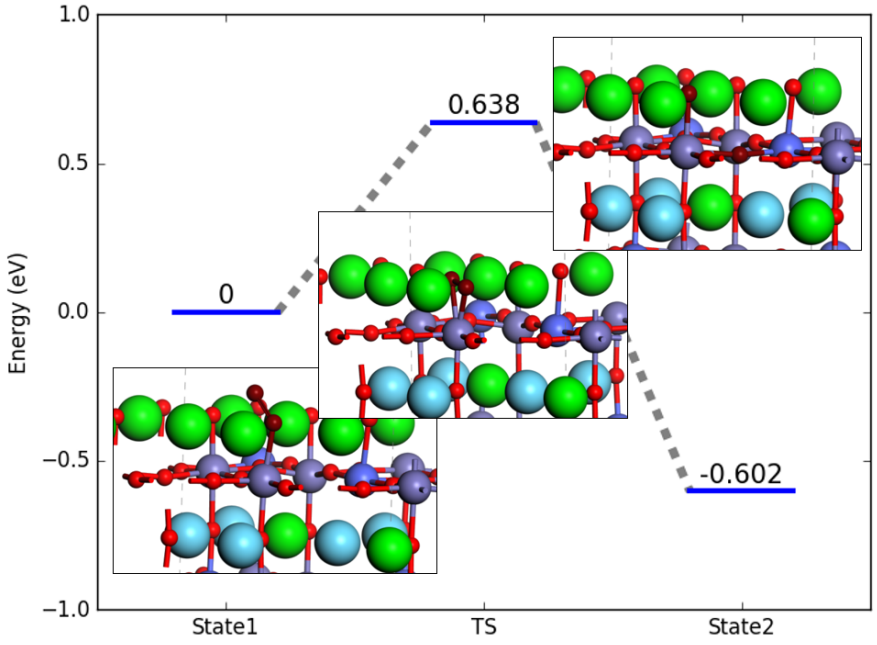

Fig. S7-3 Energy profile for reaction R3.

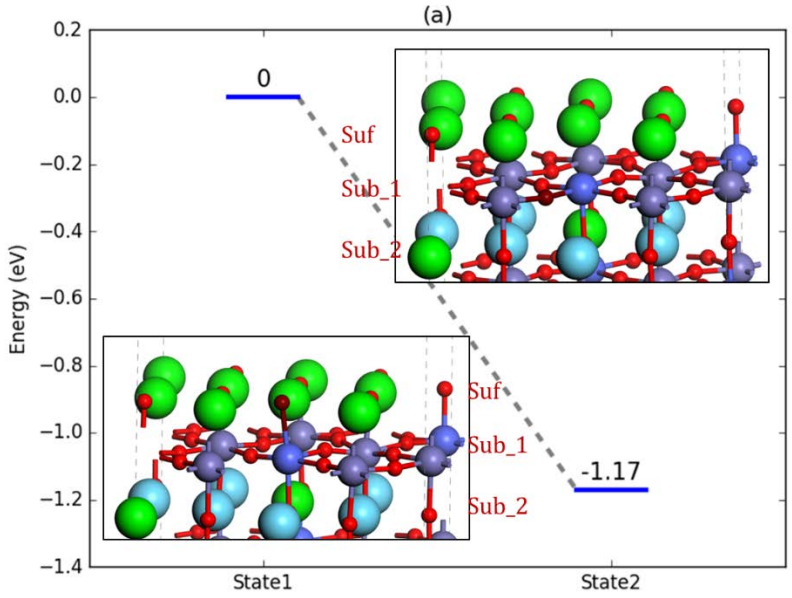
(a)
0.2
0.0
−0.2
−0.4
−0.6
−0.8
−1.0
−1.2
−1.4
Energy (eV)
0
Suf
Sub_1
Sub_2
Suf
Sub_1
Sub_2
-1.17
State1
State2

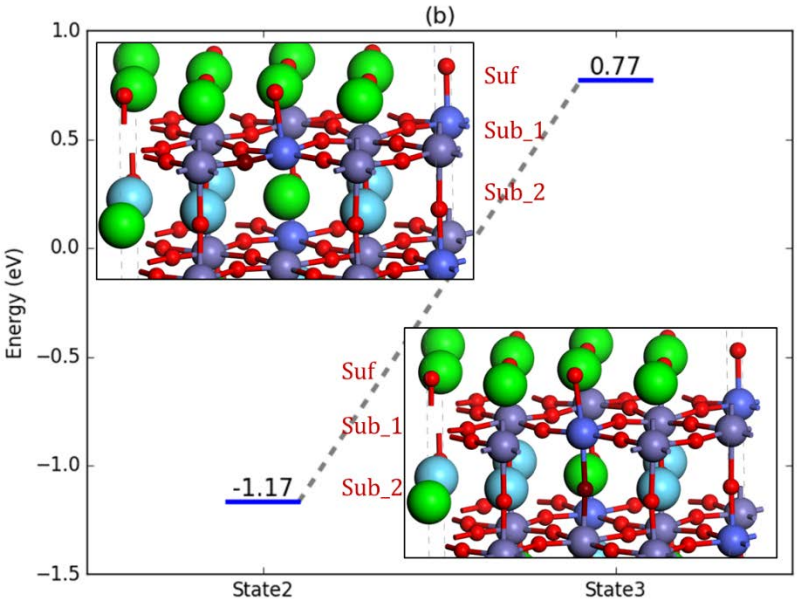
(b)
1.0
0.5
0.0
−0.5
−1.0
−1.5
Energy (eV)
Suf
Sub_1
Sub_2
0.77
Suf
Sub_1
Sub_2
-1.17
State2
State3

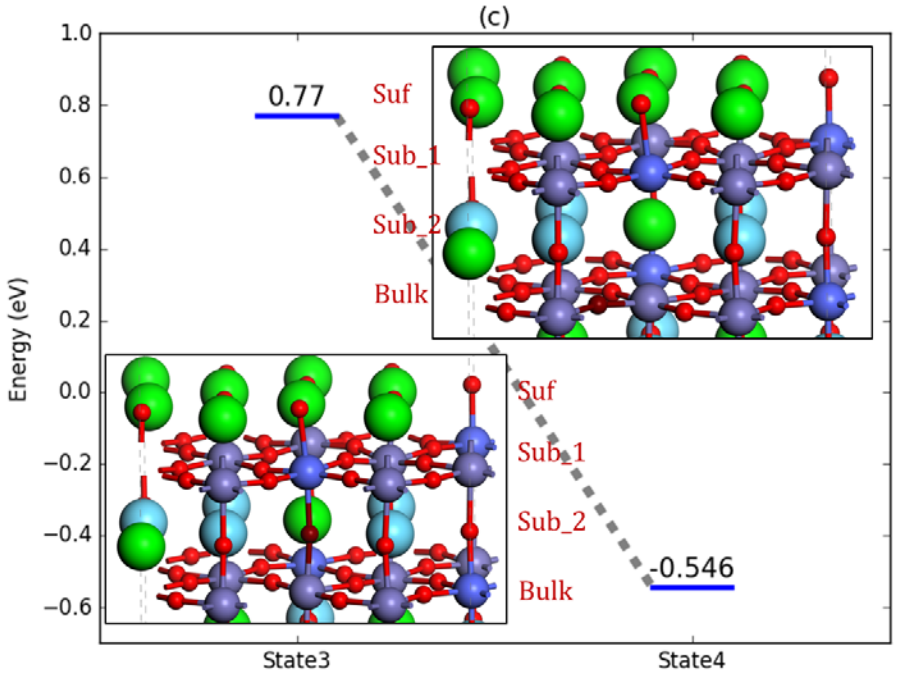

Fig. S7-4 Energy profile for reaction R4. (a) Migration of an oxide ion from the surface to the first subsurface layer. (b) Migration of an oxide ion from the first subsurface layer to the second subsurface layer. (c) Migration of an oxide ion from the second subsurface layer to the third subsurface layer.

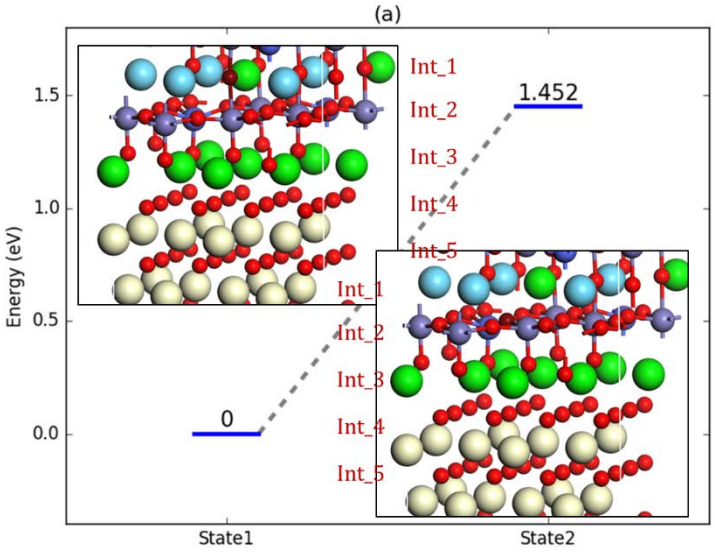
(a)
Energy (eV)
1.5
1.0
0.5
0.0
Int_1
Int_2
Int_3
Int_4
Int_5
1.452
0
State1
State2

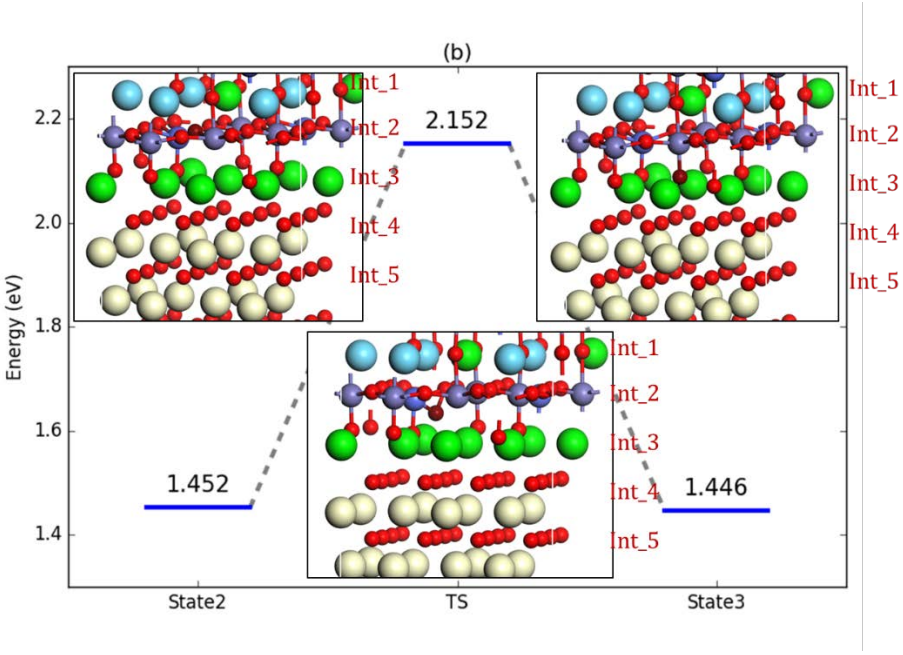
(b)
Energy (eV)
2.2
2.0
1.8
1.6
1.4
Int_1
Int_2
Int_3
Int_4
Int_5
2.152
1.452
1.446
State2
TS
State3

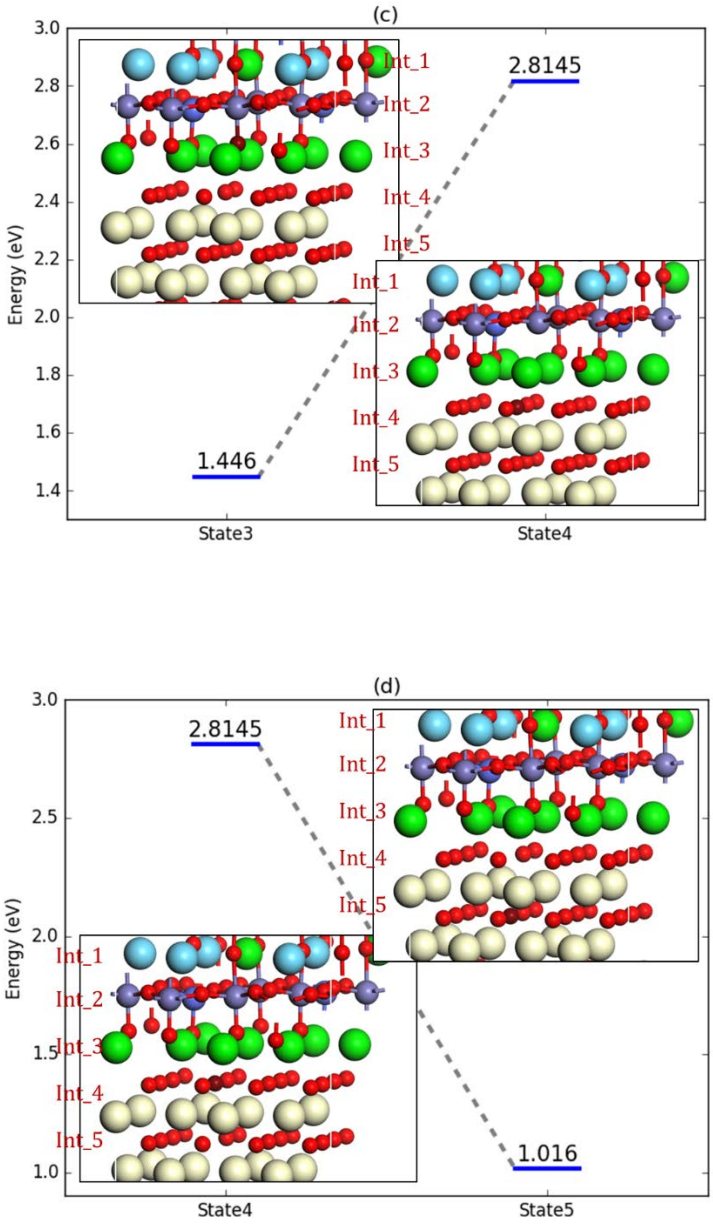

Fig. S7-5 Energy profile for reaction R5. (a) Migration of an oxide ion from the first interfacial layer to the second interfacial layer. (b) Migration of an oxide ion from the second interfacial layer to the third interfacial layer. (c) Migration of an oxide ion from the third interfacial layer to the fourth interfacial layer. (d) Migration of an oxide ion from the fourth interfacial layer to the fifth interfacial layer.

S8: Influence of vacancy concentration on reaction rate constants and diffusivities

$k^{-}_{R4\_3}$, which is the reaction rate constant for R4, and $k^{+}_{R5\_1}$, which is the reaction rate constant for R5, are modified as follows:

$$k^{-}_{R4\_3} = \frac{k_B T}{h} exp\left(-\frac{\Delta G_{k^{-}_{R4\_3}}(T)}{k_B T}\right) exp\left(-\frac{\Delta G_{k^{-}_{R4\_3}}\left(C_{V_O}\right)}{k_B T}\right)$$

$$k^{+}_{R5\_1} = \frac{k_B T}{h} exp\left(-\frac{\Delta G_{k^{+}_{R5\_1}}(T)}{k_B T}\right) exp\left(-\frac{\Delta G_{k^{+}_{R5\_1}}\left(C_{V_O}\right)}{k_B T}\right)$$

$$\Delta G_{k^{-}_{R4\_3}}\left(C_{V_O}\right) = \Delta G_{k^{+}_{R5\_1}}\left(C_{V_O}\right) = a\frac{\Delta C_{V_O}}{C^{max}_{O^{2-}}} \quad \text{(S8-1)}$$

From reference 7, the bulk diffusivity of oxide ions in LSCF and surface reaction rate constants on LSCF are all related to the pressure of oxygen gas. Through derivations, we have:

$$D_{O^{2-}} = \frac{\lambda^2}{6}\frac{k_B T}{h} exp\left(-\frac{\Delta G_{D_{O^{2-}}}(T)}{k_B T}\right) exp\left(-\frac{\Delta G_{D_{O^{2-}}}\left(C_{V_O}\right)}{k_B T}\right)$$

$$\Delta G_{D_{O^{2-}}}\left(C_{V_O}\right) = 2\gamma_{bulk} a\frac{\Delta C_{V_O}}{C^{max}_{O^{2-}}} \quad \text{(S8-2)}$$

$$k^{+}_{R3} = \frac{k_B T}{h} exp\left(-\frac{\Delta G_{k^{+}_{R3}}(T)}{k_B T}\right) exp\left(-\frac{\Delta G_{k^{+}_{R3}}\left(C_{V_O}\right)}{k_B T}\right) exp\left(-\frac{\Delta G_{k^{+}_{R3}}\left(C_{O^{-}_{suf}}\right)}{k_B T}\right)$$

$$k^{-}_{R3} = \frac{k_B T}{h} exp\left(-\frac{\Delta G_{k^{-}_{R3}}(T)}{k_B T}\right) exp\left(-\frac{\Delta G_{k^{-}_{R3}}\left(C_{V_O}\right)}{k_B T}\right) exp\left(-\frac{\Delta G_{k^{-}_{R3}}\left(C_{O^{-}_{suf}}\right)}{k_B T}\right)$$

$$\Delta G_{k^{+}_{R3}}\left(C_{V_O}\right) = \Delta G_{k^{-}_{R3}}\left(C_{V_O}\right) = 2\gamma_{suf} a\frac{\Delta C_{V_O}}{C^{max}_{O^{2-}}} \quad \text{(S8-3)}$$

The experimental values for γ_{bulk}, γ_{suf} are listed in Table S6-4.

Details on the derivation of expressions (S8-2), (S8-3) are as follows:

The equation for oxygen vacancy formation in bulk LSCF is as follows:

$$O_O'' \rightarrow V_O^x + \frac{1}{2}O_2 + 2e'$$

The relation between the concentrations of O_O'', V_O^x, O_2 and the vacancy formation energy is as follows:

$$C_{O_2}^{1/2}\frac{C_{V_O}}{C_{O^{2-}}^{max}-C_{V_O}} = exp\left(-\frac{\Delta G_{f,vac}}{k_BT}\right) = exp\left(-\frac{\Delta G_{f,vac}^{perf}+a\frac{C_{V_O}}{C_{O^{2-}}^{max}}}{k_BT}\right) \quad \text{(S8-4)}$$

$$ln\left(C_{O_2}\right) = -2\frac{\Delta G_{f,vac}^{perf}+a\frac{C_{V_O}}{C_{O^{2-}}^{max}}}{k_BT} - 2ln\left(\frac{C_{V_O}}{C_{O^{2-}}^{max}-C_{V_O}}\right) \quad \text{(S8-5)}$$

According to reference 5, the relation between oxide ion diffusivity and C_{O_2} are as follows:

$$D_{O^{2-}} = \frac{\lambda^2}{6}\frac{k_BT}{h}exp\left(-\frac{\Delta G_{D_{O^{2-}}}(T)}{k_BT}\right)exp\left(-\frac{\Delta G_{D_{O^{2-}}}\left(C_{V_O}\right)}{k_BT}\right) \propto C_{O_2}^{\gamma_{bulk}} \quad \text{(S8-6)}$$

Therefore

$$\Delta G_{D_{O^{2-}}}\left(C_{V_O}\right) = -\gamma_{bulk}k_BT\,ln\left(C_{O_2}\right) + const \quad \text{(S8-7)}$$

After putting (S8-5) into (S8-7), we have

$$\Delta G_{D_{O^{2-}}}\left(C_{V_O}\right) = 2\gamma_{bulk}(\Delta G_{f,vac}^{perf} + a\frac{C_{V_O}}{C_{O^{2-}}^{max}}) + 2\gamma_{bulk}k_BTln(\frac{C_{V_O}}{C_{O^{2-}}^{max}-C_{V_O}}) + const \quad \text{(S8-8)}$$

Since $2\gamma_{bulk}\Delta G_{f,vac}^{perf}$ term is a constant (not a function of concentration), and $\gamma_{bulk}k_B\,Tln\left(\frac{C_{V_O}}{C_{O^{2-}}^{max}-C_{V_O}}\right) \ll \gamma_{bulk}a\frac{C_{V_O}}{C_{O^{2-}}^{max}}$, we have

$$\Delta G_{D_{O^{2-}}}(C_{V_O}) = 2\gamma_{bulk} a \frac{C_{V_O}}{C_{O^{2-}}^{max}} + const \quad \text{(S8-9)}$$

Considering that in equilibrium, $\Delta G_{D_{O^{2-}}}(C_{V_O}) = 0$, we have

$$\Delta G_{D_{O^{2-}}}(C_{V_O}) = 2\gamma_{bulk} a \frac{\left(C_{V_O} - C_{V_O}^{equi}\right)}{C_{O^{2-}}^{max}} = 2\gamma_{bulk} a \frac{\Delta C_{V_O}}{C_{O^{2-}}^{max}} \quad \text{(S8-2)}$$

Where $C_{V_O}^{equi}$ is the vacancy concentration in bulk LSCF in equilibrium, which is about 600 mol/m^3.

The relation between k_{R3}^{+}, k_{R3}^{-} and C_{O_2} are as follows:

$$k_{R3}^{+}, k_{R3}^{-} \propto C_{O_2}^{\gamma_{suf}}$$

After derivations similar to expressions (S8-6)~(S8-8), we have

$$\Delta G_{k_{R3}^{+}}(C_{V_O}) = \Delta G_{k_{R3}^{-}}(C_{V_O}) = 2\gamma_{suf} a \frac{C_{V_O}}{C_{O^{2-}}^{max}} + const \quad \text{(S8-10)}$$

Considering that when $C_{V_O} = C_{V_O}^{DFT}$, $k_{R3}^{+} = \frac{k_B T}{h} exp\left(-\frac{\Delta G_{k_{R3}^{+}}(T)}{k_B T}\right)$, $\mathrm{k_{R3}^{-}} = \frac{k_B T}{h} exp\left(-\frac{\Delta G_{k_{R3}^{-}}(T)}{k_B T}\right)$, we have

$$\Delta G_{k_{R3}^{+}}(C_{V_O}) = \Delta G_{k_{R3}^{-}}(C_{V_O}) = 2\gamma_{suf} a \frac{\left(C_{V_O} - C_{V_O}^{DFT}\right)}{C_{O^{2-}}^{max}} = 2\gamma_{suf} a \frac{\Delta C_{V_O}}{C_{O^{2-}}^{max}} \quad \text{(S8-3)}$$

Where $C_{V_O}^{DFT}$ is the vacancy concentration in bulk LSCF used in the DFT calculations, which is about 1154 mol/m^3.

References

(1) P. Atkins, J. D. Paula, Physical Chemistry, 9st Edition; Oxford University Press, 2010.

(2) C. T. Campbell, J. R. V. Sellers, The Entropies of Adsorbed Molecules. J. Am. Chem. Soc. 2012, 134, 18109.

(3) C. T. Campbell; J. R. V. Sellers, Enthalpies and Entropies of Adsorption on Well-Defined Oxide Surfaces: Experimental Measurements. Chem. Rev. 2013, 113, 4106−4135.

(4) S. Suthirakun, S. C. Ammal, A. B. Muñoz-García, G. Xiao, F. Chen, H.-C. z. Loye, E. A. Carter, A. Heyden, Theoretical Investigation of H2 Oxidation on the Sr2Fe1.5Mo0.5O6 (001) Perovskite Surface under Anodic Solid Oxide Fuel Cell Conditions. J. Am. Chem. Soc. 2014, 136, 8374−8376.

(5) J. A. Lane, S. J. Benson, Oxygen Transport in $La_{0.6}Sr_{0.4}Co_{0.2}Fe_{0.8}O_{3-\delta}$. Solid State Ionics 1999, 121, 201−208.

(6) J. Laurencin, M. Hubert, K. Couturier, T. Le Bihan, P. Cloetens, F. Lefebvre-Joud, E. Siebert, Reactive Mechanisms of LSCF Single-phase and LSCF-CGO Composite Electrodes Operated in Anodic and Cathodic Polarisations. Electrochimica Acta 2015, 174, 1299-1316.

(7) J. A. Lane, S. J. Benson, Oxygen Transport in $La_{0.6}Sr_{0.4}Co_{0.2}Fe_{0.8}O_{3-\delta}$. Solid State Ionics 1999, 121, 201−208.

(8) M. Kuhn, Y. Fukuda, S. Hashimoto, K. Sato, K. Yashiro, J. Mizusaki, Oxygen Nonstoichiometry and Thermo-Chemical Stability of Perovskite-Type $La_{0.6}Sr_{0.4}Co_{1-y}Fe_yO_{3-\delta}$ (y= 0, 0.2, 0.4, 0.5, 0.6, 0.8, 1). Materials. J. Electrochem. Soc. 2013, 160, F34−F42.

(9) G. M. Rupp, A. Schmid, A. Nenning, J. Fleig The Superior Properties of $La_{0.6}Ba_{0.4}CoO_{3-\delta}$ Thin Film Electrodes for Oxygen Exchange in Comparison to $La_{0.6}Sr_{0.4}CoO_{3-\delta}$. J. Electrochem. Soc. 2016, 163, F564−F573.

(10) F. S. Baumann, J. Fleig, H.-U. Habermeier, J. Maier, Impedance Spectroscopic Study on

Well-defined (La,Sr)(Co,Fe)$O_{3-\delta}$ model electrodes. Solid State Ionics 2006, 177, 1071-1081.